Theory of the special Smith-Purcell radiation from a rectangular grating

Weihao Liu' , Weiwei Li, Zhigang He' , and Qika Jia

Citation: AIP Advances **5**, 127135 (2015); doi: 10.1063/1.4939538
View online: http://dx.doi.org/10.1063/1.4939538
View Table of Contents: http://aip.scitation.org/toc/adv/5/12
Published by the American Institute of Physics

Articles you may be interested in

Investigation on the special Smith-Purcell radiation from a nano-scale rectangular metallic grating
AIP Advances **6**, 035202035202 (2016); 10.1063/1.4943502

A multimode terahertz-Orotron with the special Smith–Purcell radiation
AIP Advances **108**, 183510183510 (2016); 10.1063/1.4949015

A compact terahertz free-electron laser with two gratings driven by two electron-beams
AIP Advances **24**, 023109023109 (2017); 10.1063/1.4976122

Graphene on nanoscale gratings for the generation of terahertz Smith-Purcell radiation
AIP Advances **105**, 241102241102 (2014); 10.1063/1.4904264

Numerical modeling of a table-top tunable Smith–Purcell terahertz free-electron laser operating in the super-radiant regime
AIP Advances **96**, 151502151502 (2010); 10.1063/1.3386543

Superradiant terahertz Smith-Purcell radiation from surface plasmon excited by counterstreaming electron beams
AIP Advances **90**, 031502031502 (2007); 10.1063/1.2432270

Theory of the special Smith-Purcell radiation from a rectangular grating

Weihao Liu,[1,a] Weiwei Li,[1,2] Zhigang He,[1,b] and Qika Jia[1]
[1]*National Synchrotron Radiation Laboratory, University of Science and Technology of China, Hefei, Anhui, 230029, China*
[2]*Istituto Nazionale di Fisica Nucleare, Laboratori Nazionali di Frascati, via E. Fermi 40, 00044 Frascati, RM, Italy*

(Received 19 October 2015; accepted 21 December 2015; published online 30 December 2015)

The recently uncovered special Smith-Purcell radiation (S-SPR) from the rectangular grating has significantly higher intensity than the ordinary Smith-Purcell radiation (SPR). Its monochromaticity and directivity are also much better. Here we explored the mechanism of the S-SPR by applying the fundamental electromagnetic theory and simulations. We have confirmed that the S-SPR is exactly from the radiating eigen modes of the grating. Its frequency and direction are well correlated with the beam velocity and structure parameters, which indicates its promising applications in tunable wave generation and beam diagnostic. © *2015 Author(s). All article content, except where otherwise noted, is licensed under a Creative Commons Attribution (CC BY) license (http://creativecommons.org/licenses/by/4.0/).*
[http://dx.doi.org/10.1063/1.4939538]

I. INTRODUCTION

Smith-Purcell radiation (SPR), occurring as charged particles passing over a periodic surface,[1–6] was one of the hottest research topics in the twentieth century. Even to the present, it has still received much attentions for its potential in generating terahertz wave radiation,[7,8] which can not be easily obtained by other methods.[9–14] The rectangular gratings are commonly used to get the SPR in these applications.[15,16] As is known, the ordinary Smith-Purcell radiation (O-SPR) from grating is a broad spectra emission which extends to all directions above the grating.[17] The radiation wavelength and direction satisfy the following famous relation:

$$\lambda = -\frac{L}{n}\left(\frac{1}{\beta} - \cos\theta\right), \tag{1}$$

where λ is radiation wavelength, L is the structural period, n is a negative integer, β is the ratio of beam velocity to light speed, and θ denotes the radiation direction.

Recently, an interesting special kind of Smith-Purcell radiation (S-SPR) from the rectangular grating was uncovered in Ref. 18. By simply reducing the groove width of the grating (see Fig. 1), a monochromaticity radiation with much higher intensity in specified direction was obtained by simulations. Yet in Ref. 18, the detailed theoretical analyses were not carried out. To better understand this radiation and to find its possible applications, in the present paper we further explore the mechanism and requirement of the S-SPR. By analyzing the dispersion and radiation characteristics, we find that the S-SPR is exactly from the radiating eigen modes of the grating. In mechanism, it is similar to the exotic enhanced SPR from the photonic crystals (PhCs),[19,20] which is generated from the photonic band (PB) modes of the PnCs excited by electron beam. As is known that the PhCs based SPR can generate narrow-band radiation with intensity orders higher than that from an ordinary grating.[21]

[a]Electronic mail: liuwhao@ustc.edu.cn
[b]Electronic mail: hezhg@ustc.edu.cn

 ©Author(s) 2015.

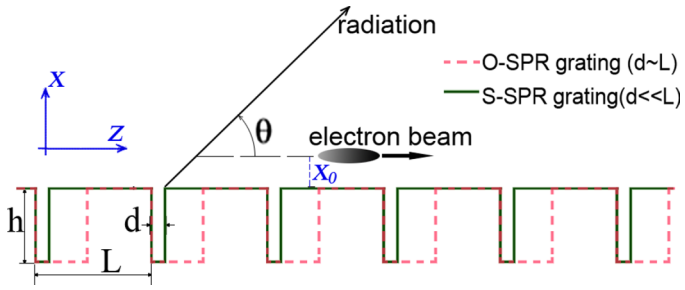

FIG. 1. Schematic diagram of the SPR from a rectangular grating excited by uniformly moving electron beam.

While we will show that, for the S-SPR, the radiating eigen modes are just as the PBs which essentially lead to the enhancement. In other words, by properly adjusting the grating parameters and beam velocity, the exotic enhanced SPR can also be achieved in an ordinary grating, which is demonstrated for the first time to our knowledge. Obviously, compared with the PnCs, the rectangular grating is much simpler for experiments. Its remarkable advantages in intensity, tunability, and simpleness in structure make it a promising way for tunable wave generation and beam energy diagnostic.

The paper is organized as follows: section II presents the derivation of the theoretical formulas; section III analyzes the dispersion characteristics of the eigen modes in the grating; the mechanism and requirements of the S-SPR are explored in section IV, where the possible applications are also discussed; section V is the conclusion.

II. DERIVATION OF THE FORMULAS

The schematic diagram of the problem that we are going to analyze is shown in Fig. 1, in which an electron beam passes over a conductor grating with rectangular grooves. It is well known that the electron beam will excite the resonator modes in the grooves and the diffraction radiation in the upper half-space. The mode matching method can be used to handle the problem.

In the Cartesian coordinate system shown in the figure, the induced electric field in z-direction (E_z component) by the electron beam should satisfy the following non-homogeneous equation[22]:

$$\frac{\partial^2 E_z^i}{\partial x^2} + \frac{\partial^2 E_z^i}{\partial z^2} - \frac{1}{c^2}\frac{\partial^2 E_z^i}{\partial t^2} = \frac{1}{\varepsilon_0}\frac{\partial \rho}{\partial z} + \mu_0 \frac{\partial J_z}{\partial t}, \tag{2}$$

where c is the light speed in vacuum, ε_0 and μ_0 are respectively the permittivity and permeability of the vacuum. ρ and J_z respectively denote the charge density and current density, and for the line electron beam with quantity of q and velocity of v, they can be expressed as[22]:

$$\rho = q\delta(x - x_0)\delta(z - vt), \tag{3}$$

$$J_z = qv\delta(x - x_0)\delta(z - vt), \tag{4}$$

where x_0 denotes the x-directional position of the electron beam as shown in the figure. Note that here we only consider the 2D model, in which the y-directional dependences are ignored.

With the help of Fourier transformation method, Eq. (2) can be solved and the E_z component with circular frequency ω can be obtained:

$$E_z^i = \frac{\omega\mu q}{4\pi k_c}\left(\frac{1}{\beta^2} - 1\right)e^{-jk_c|x-x_0| - jk_z z}, \tag{5}$$

where $k_c = \sqrt{k_0^2 - k_z^2} = \sqrt{(\frac{\omega}{c})^2 - (\frac{\omega}{v})^2}$. Applying the Maxwell equations, other field components of the induced waves can be obtained:

$$\begin{cases} E_x^i = s\dfrac{k_z}{k_c^2}\dfrac{\omega\mu q}{4\pi}\left(\dfrac{1}{\beta^2}-1\right)e^{-jk_c(x-x_0)-jk_z z} \\ H_y^i = s\dfrac{\omega\varepsilon}{k_c^2}\dfrac{\omega\mu q}{4\pi}\left(\dfrac{1}{\beta^2}-1\right)e^{-jk_c(x-x_0)-jk_z z} \end{cases}, \tag{6}$$

where $s = -1$ for $x > x_0$ and $s = 1$ for $x < x_0$.

The induced waves will be diffracted in the upper half-space of the grating. To satisfy the periodic boundary conditions of the grating, the diffraction waves should be expanded into infinite space harmonics[23]:

$$\begin{cases} E_z^I = \displaystyle\sum_{n=-\infty}^{\infty} A_n e^{-k_{xn}x}e^{-jk_{zn}z} \\ E_x^I = \displaystyle\sum_{n=-\infty}^{\infty} A_n \frac{-jk_{zn}}{k_{xn}} e^{-k_{xn}x}e^{-jk_{zn}z} \\ H_y^I = \displaystyle\sum_{n=-\infty}^{\infty} A_n \frac{-j\omega\varepsilon}{k_{xn}} e^{-k_{xn}x}e^{-jk_{zn}z} \end{cases}, \tag{7}$$

where $k_{xn} = \sqrt{k_{zn}^2 - k_0^2}$, $k_{zn} = k_z + \frac{2n\pi}{L}$, and $A_n s$ are the coefficients to be determined by boundary conditions. Note that if $k_{zn} > k_0$, k_{xn} is real, which means that the diffraction waves are evanescent in the x-direction and can not radiate into space; while if $k_{zn} < k_0$, k_{xn} is imaginary, signifying the diffraction waves can radiate into upper half-space. Readily to find that only the negative harmonic waves ($n < 0$) can radiate. The radiation wavelength and direction should satisfy the SPR relation of Eq. (1).

As for the resonator modes in the grooves, we consider the case that the groove width is much less than the radiation wavelength. Then the fields in the grooves can be expressed as the transverse electric and magnetic (TEM) mode in the x-direction[23]:

$$\begin{cases} E_z^{II} = C\dfrac{\sin[k_0(h+x)]}{\sin(k_0 h)} \\ H_y^{II} = C\dfrac{-j\omega\varepsilon}{k_0}\dfrac{\cos[k_0(h+x)]}{\sin(k_0 h)} \end{cases}. \tag{8}$$

The incident waves, diffraction waves, and the resonator modes presented above should satisfy the the following mode matching conditions at the groove aperture[23]:

$$\begin{cases} E_z^i\big|_{x=0} + E_z^I\big|_{x=0} = E_z^{II}\big|_{x=0}, \quad -d/2 < z < d/2 \\ \displaystyle\int_{-d/2}^{d/2} \left(H_y^i\big|_{x=0} + H_y^I\big|_{x=0}\right)dx = \int_{-d/2}^{d/2} H_y^{II}\big|_{x=0}dx \end{cases}. \tag{9}$$

Substituting Eqs. (6)-(8) into Eq. (9) and doing complicate but straightforward arithmetical operation, coefficients ($A_n s$) of the diffraction waves can be solved. The radiation power per unit angle can then be obtained by:

$$\frac{dP}{d\theta} = \sum_{n=-\infty}^{n=\infty} \frac{\int_{-d/2}^{d/2} S_{xn}(\theta_n)dz}{\sin\theta_n}, \tag{10}$$

where $S_{xn}(\theta_n)$ is the Poynting vector of the radiation wave with the n-th harmonic order:

$$S_{xn}(\theta_n) = \frac{E_{zn}^I H_{yn}^{I\,*}}{-2} = |A_n|^2\frac{\omega\varepsilon}{\tau_n}. \tag{11}$$

Here '$*$' is the conjugate operator and $\tau_n = jk_{xn}$. For most cases, the first negative space harmonic ($n = -1$) dominants the diffraction wave. So we only consider the n $= -1$ component, Eq. (10) is then simplified as:

$$\left.\frac{dP}{d\theta}\right|_{n=-1} = \frac{\omega\varepsilon L}{\tau_{-1}\sin\theta_{-1}}|A_{-1}|^2 \tag{12}$$

The detailed calculations will be given in the following sections.

III. INVESTIGATION ON THE EIGEN MODES OF THE GRATING

The eigen modes of the grating plays the essential role in determining the diffraction characteristics. Yet in almost all previous literatures about the grating, only the evanescent eigen modes were considered, the radiating eigen modes have never been investigated to our knowledge. It may be because the gratings were most commonly used as slow wave structure, where only the surface modes were applied to interact with the electron beam.[16] In order to find the mechanism of the S-SPR and to illustrate the differences between the O-SPR and the S-SPR, here we will specifically analyze the radiating eigen modes of the grating.

As is known that the characteristics of the electromagnetic modes in the grating are governed by the dispersion equation, which can be derived by letting the incident fields vanish in Eq. (9):

$$\frac{Ld}{4}\sum_{n=-\infty}^{\infty}\frac{k_{zn}^2 k_{xn}}{\sin^2(k_{zn}d/2)} = k_0\tan k_0 h. \tag{13}$$

In calculations, we keep the period L to be 1 mm, and gradually changing the width and depth of the rectangular grooves (change the values of d/L and h/L). The calculated dispersion curves in Brillouin diagram are shown in Fig. 2. Here only the fundamental modes are considered because they are the dominant modes in radiation. The subplots (a)-(d) respectively denote the cases that h/L is 0.5, 0.4, 0.3, and 0.2. The curves in the shadow regions denote the slow waves or surface modes bounding to the grating. Other curves signify the radiation modes. We can see that when the groove depth or groove width is relatively large, see the cases that $h/L \geq 0.4$ or $d/L \geq 0.2$ in the figure, both the surface modes and radiation modes can exist in the grating. While as both the groove depth and groove width are very small, the surface modes can not exist, see the cases d/L = 0.05 in subplots (c) and (d). The reasons for this will be illustrated as below.

In physics, the electromagnetic energy of the resonator modes in the rectangular grooves will 'outflow' through the groove apertures. They can radiate into the upper half-space or 'inflow' to adjacent resonators. When an array of resonator modes 'outflow' successively, they will couple with each other. The intercoupling of the radiation part leads to the radiation modes in the upper half-space, while that of the 'interflow' part leads to the surface modes in the grating. Both the radiation modes and surface modes can independently satisfy the grating's boundary conditions, namely, they can independently exist in the grating. When the groove width is reduced, the distance between the adjacent resonators will be increased, which weakens or even eliminates the 'interflow' coupling of the resonator modes. The surface modes will no longer exist when the 'interflow' coupling is completely eliminated. This is just the reason for the absence of surface modes in the grating with very narrow grooves. As for the quite shallow grooves (like a planar surface), they can hardly sustain any resonator modes for coupling. Readily to understand that neither surface modes nor radiation modes can exist under this condition.

An phenomenon signifying the coupling is the slopes of dispersion curves. As is known that the dispersion curves of the resonator modes are a group of horizontal lines with discrete resonator frequencies.[24] The group velocity of resonator modes is zero, i.e., they can not propagate along the grating. The coupling will cause the dispersion curves to bend, namely, the frequencies of both the surface modes and radiating modes will deviate from the resonator ones because of the coupling. And a stronger coupling leads to a larger deviation. This is exactly the reason why the gratings with narrower grooves have flatter dispersion curves as shown in the figure. The periodically changing of the slopes stems from the periodicity of grating. For the surface modes, the slopes signify that the group velocities of waves are in forward or backward direction along the grating.

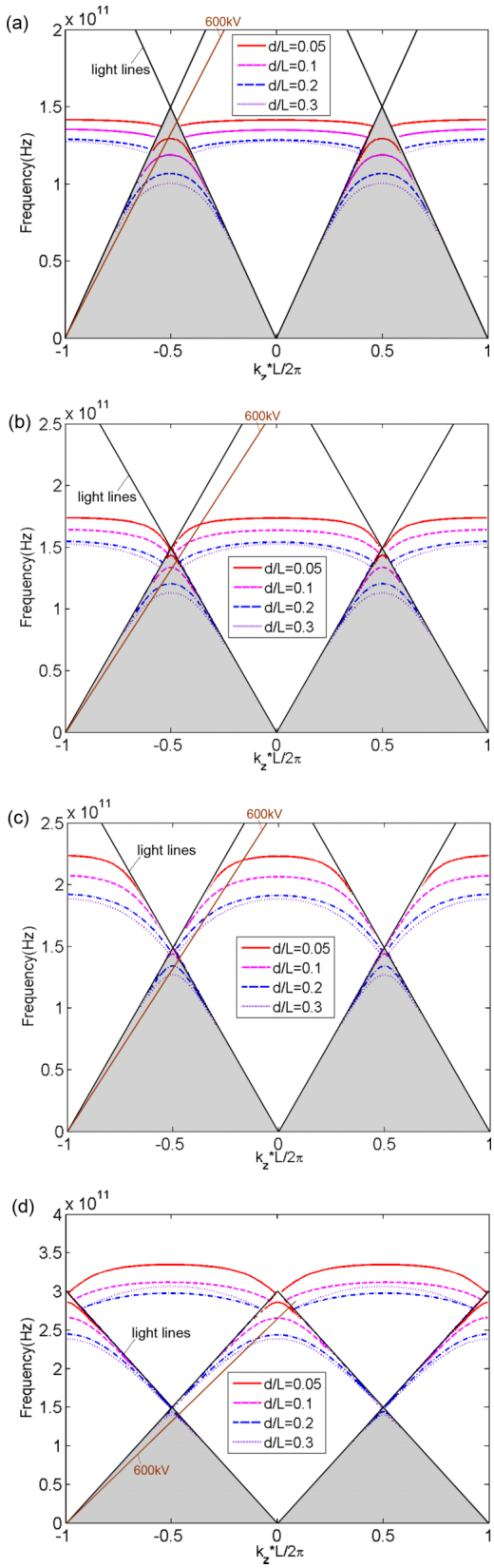

FIG. 2. Calculated dispersion curves for different grating parameters: (a) h = 0.5 mm, (b) h = 0.4 mm, (c) h = 0.3 mm, (d) h = 0.2 mm. In all figures, the grating period is L = 1 mm.

IV. RADIATION CHARACTERIZATION—THEORETICAL CALCULATION AND SIMULATIONS

In this section we calculate the diffraction radiations from the grating by applying the formulas derived in section II. We will specifically investigate the differences between the O-SPR and the S-SPR. Then based on the analyses in section III we will uncover the mechanism of the S-SPR. In calculations, we set the charge quantity and the acceleration voltage of the exciting beam to be 10^{-12} C and 600 kV, respectively. Structure parameters follow that given in section III. The calculated results of the radiation spectrums are shown in Fig. 3, in which the subplots (a)-(d) respectively denote the cases that h/L is 0.5, 0.4, 0.3, and 0.2, following that given in Fig. 2.

When the groove depth or groove width is relatively large, the radiation spectrums will cover a broad frequency band (without obvious radiation peaks), see the cases that $h/L = 0.5$ or $d/L \geq 0.2$ in the figure. Under these conditions, the radiation waves will extend to a wide range of directions in the upper half-space, which is the typical feature of the O-SPR. While as both the groove depth and groove width are relatively small, the radiation intensities will reach sharp peaks at a certain frequencies, see the cases d/L = 0.05 in subplots (c) and (d). Under these conditions, the radiation waves will largely focused in the directions specified by Eq. (1), which are exactly the features of the S-SPR.[18] We can observe that the radiation intensities of the S-SPR are an order of magnitude higher than that of the O-SPR when other parameters are the same.

To find the mechanism of the S-SPR, we reexamine the dispersion curves given in Fig. 2. It shows that the 600 kV beam line will intersect with the dispersion curves of the eigen modes of the grating, indicating that these modes will be excited by the electron beam. When the groove depth or groove width is relatively large, the surface modes will primarily be excited to interact with the electron beam, which is similar to the beam-wave interaction in the traditional vacuum electronics.[16,25] Under these conditions, the radiation modes can not be effectively excited even though the beam line may intersect with the radiation modes (as the intensity of the surface modes is much higher than that of the radiation modes). The radiation here is merely from the grating's reflection to the evanescent incident wave of the electron beam, which is exactly the O-SPR.[22] While as both the groove depth and groove width are relatively small, the surface modes can not be excited because the beam line does not intersect with the surface modes or because the surface modes actually don't exist as mentioned above (see the cases d/L = 0.05 in Fig. 2(c) and Fig. 2(d)). Under these conditions, the radiation modes can effectively interact with the electron beam. Namely, they will be excited to generate radiation, and the radiation frequency is just the frequencies of the intersections. Examinations show that the frequencies of the radiation modes coincide well with the peak frequencies of the S-SPR. So we can confirm that the S-SPR is exactly from the radiation eigen modes of the grating excited by electron beam. From the above analyses, we can see that the following requirements should be satisfied to get the S-SPR: the surface modes have not been excited, and simultaneously, the radiation modes have been excited. To meet these requirements, the structure parameters of the grating and the beam velocity should be set properly.

It is worth noting that the mechanism of the S-SPR presented above is similar to that of the exotic radiation from the PhCs,[19,20] in which electron beam excites the PB modes of the PnCs to generate the narrow-band radiation with peak intensity orders higher than that from an ordinary grating. Examinations revealed that the excited radiation eigen modes of the S-SPR from the grating are just as the PBs which essentially lead to the remarkable enhancement. So we have demonstrated, for the first time, that the exotic enhanced radiation can also be found in an ordinary grating with structure parameter well adjusted. Also note that another similar phenomenon was given in Ref. 26, which coupled the guided mode in a purpose-designed metamaterial structure into radiation. That structure was achieved by introducing an additional periodicity to an ordinary one-dimensional metal strips array. Readily to find that the physics presented in our present paper is more general and the structure is much simpler to obtain in experiments. Actually, Ref. 26 had not realized that the radiation eigen modes of an ordinary grating can also enhance the O-SPR.

Now we discuss the applications of the S-SPR. From the above results we can see that the S-SPR has great advantages in intensity, monochromaticity, and directivity over the O-SPR, which makes it a promising way for light generation, especially that can not be easily obtained by other methods, such

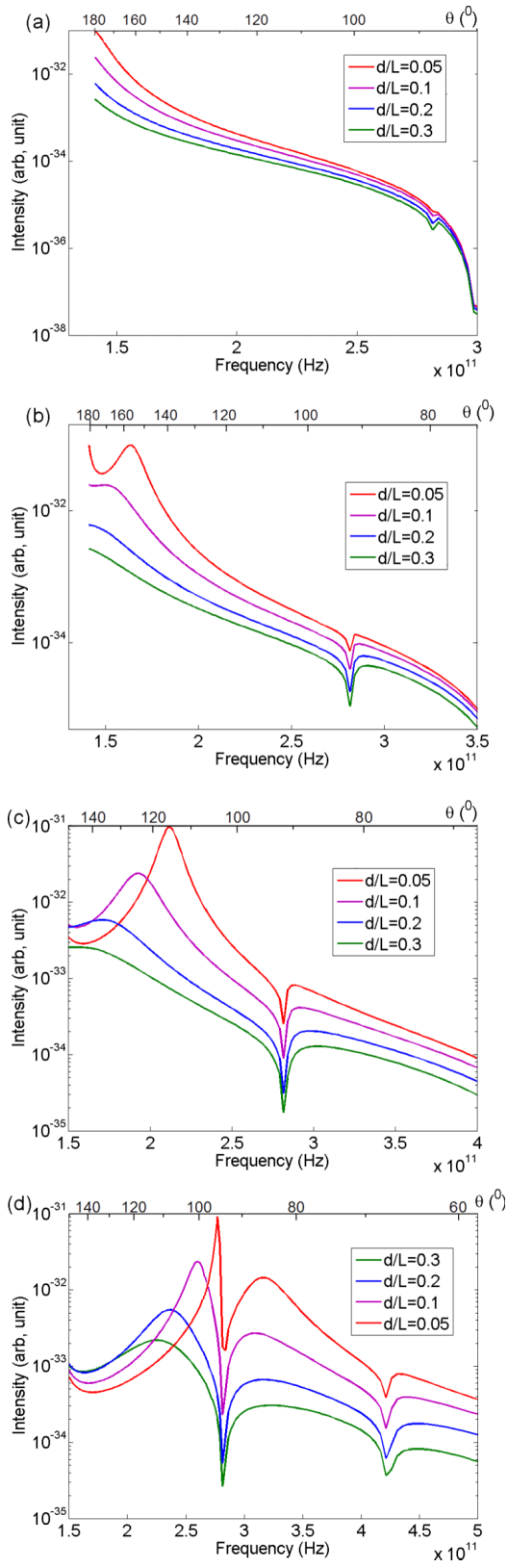

FIG. 3. Calculated radiation spectrums for different grating parameters: (a) h = 0.5 mm, (b) h = 0.4 mm, (c) h = 0.3 mm, (d) h = 0.2 mm. In all figures, the grating period is L = 1 mm. The corresponding radiation directions are shown as the upper-abscissas.

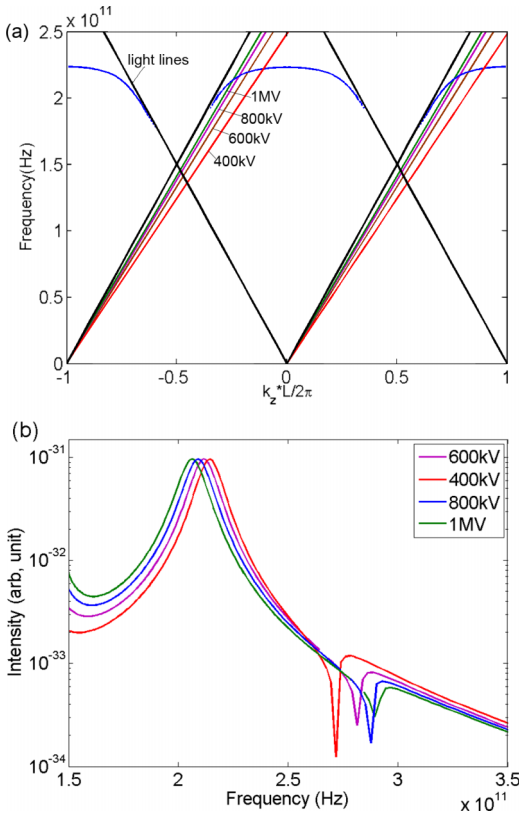

FIG. 4. Calculated dispersion curve (a) and radiation spectrums (b) for different excitation beam voltages. Here the grating parameters are: a = 0.05 mm, h = 0.3 mm, and L = 1 mm.

as terahertz radiation. Additionally, we will show that it is also a tunable radiation. From the dispersion curves shown in Fig. 2, the frequencies of the radiation modes are determined by the grating parameters and beam velocity, which offers the base of tunable light generation. The beam based tuning (electrical tuning) will be considered here. To get the optimum radiation intensity and tunability, we choose the structure parameters to be: L = 1 mm, d = 0.05 mm (d/L = 0.05), h = 03 mm (h/L = 0.3), and change the beam voltage from 400 kV to 1 MV. The dispersion curves of the radiating modes and the radiation spectrums for different beam voltages are shown in Fig. 4. The radiation frequencies from the electron beam with voltage of 400 kV, 600 kV, 800 kV, and 1 MV are respectively 214 GHz, 211 GHz, 208 GHz, and 206 GHz, corresponding to the coupling frequencies of beam lines with dispersion curve. We can observe that the relative tunable range is about 5%.

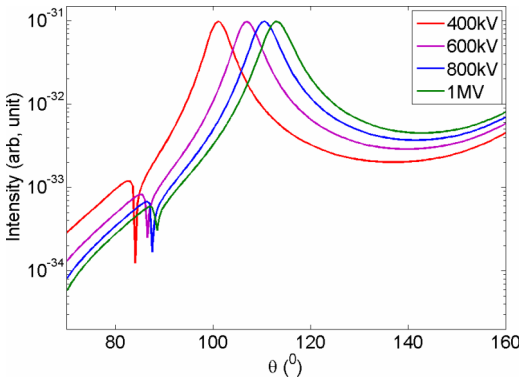

FIG. 5. Angular distributions of radiation. The grating parameters are the same as that in Fig. 4.

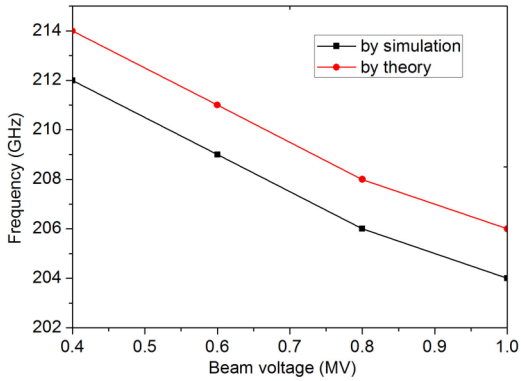

FIG. 6. Comparisons between simulation results and theoretical results. Here the grating parameters are the same as that given in Fig. 4.

Another promising application of the S-SPR is the measurement of beam energy. The radiation directions versus the beam energies are calculated in Fig. 5, in which the grating parameters follow that given above. The radiation directions from the beam with voltage of 400 kV, 600 kV, 800 kV, and 1 MV are respectively 101^0, 107^0, 110.5^0, and 113^0 (we have confirmed that the radiation frequencies, beam velocities, and the radiation directions for all cases satisfy the SPR relation). Namely, the radiation direction has the one-to-one correspondence with the beam energy. So by measuring the radiation direction of the S-SPR, the beam energy can be determined.

To verify the theoretical results, we have performed the simulations by applying the fully electromagnetic particle-in-cell (PIC) code.[27] The simulation conditions follows that given in Ref. 18, and the grating parameters are the same as that given in Fig. 4. The comparisons for the theoretical and simulation results of the radiation frequencies from different beam voltage are shown in Fig. 6. We can observe that the relative errors for all beams are less than 1%, which indicates the reasonable agreements have been achieved.

V. CONCLUSION

The special Smith-Purcell radiation from a grating with rectangular grooves was studied by applying the fundamental electromagnetic theory and simulations. The mechanism and the requirement of this radiation were explored. We have found that the S-SPR is from the radiating eigen modes of a grating excited by an electron beam. Its promising applications in the tunable wave generation and beam energy diagnostic were discussed.

ACKNOWLEDGMENTS

This work is supported by Natural Science Foundation of China (Grants No. 61471332 and No. 11205152), Anhui Provincial Natural Science Foundation (Grant No. 1508085QF113), and Fundamental Research Funds for the Central Universities under Contract No. WK2310000047.

[1] S. J. Smith and E. M. Purcell, Phys. Rev. **92**, 1069-1070 (1953).
[2] S. E. Korbly, A. S. Kesar, J. R. Sirigiri, and R. J. Temkin, Phys. Rev. Lett. **94**, 054803 (2005).
[3] O. Haeberlé, P. Rullhusen, J.-M. Salomé, and N. Maene, Phys. Rev. E **55**, 4675 (1997).
[4] J. Urata, M. Goldstein, M. F. Kimmitt, A. Naumov, C. Platt, and J. E. Walsh, Phys. Rev. Lett. **80**(3), 516-519 (1998).
[5] S. Taga, K. Inafune, and E. Sano, Opt. Express **15**(24), 16222-16229 (2007).
[6] H. L. Andrews, C. A. Brau, and J. D. Jarvis, Phys. Rev. Special Topics **8**, 110702 (2005).
[7] A. Okajima and T. Matsui, Opt. Express **22**(14), 17490-17496 (2014).
[8] K. Tantiwanichapan, X. Wang, A. K. Swan, and R. Paiella, Appl. Phys. Let. **105**, 241102 (2014).
[9] S. Son, S. J. Moon, and J. Y. Park, Opt. Let. **38**(22), 4578-4580 (2013).
[10] C. S. Martorell, V. L. Domínguez, G. A. Garofalo, A. R. Sanchez, J. Palacios, and J. Tejada, Opt. Exp. **21**(15), 17800-17805 (2013).
[11] R. Eichholz, H. Richter, M. Wienold, L. Schrottke, R. Hey, H. T. Grahn, and H.-W. Hübers, Opt. Express **21**(26), 32199-32206 (2013).

[12] H. He and X.-C. Zhang, Appl. Phys. Lett. **100**, 061105 (2012).
[13] W. Liu and Z. Xu, J. Appl. Phys. **115**, 014503 (2014).
[14] W. Liu, S. Gong, Y. Zhang, J. Zhou, P. Zhang, and S. liu, J. Appl. Phys. **111**, 063107 (2012).
[15] M. Cao, W. Liu, Y. Wang, and K. Li, Phys. Plasmas **21**, 023116 (2014).
[16] M. Cao, W. Liu, Y. Wang, and K. Li, J. Appl. Phys. **116**, 103104 (2014).
[17] P. M. van den Berg, J. Opt. Soc. Am. **64**, 325-328 (1974).
[18] W. Liu and Z. Xu, New J. Phys. **16**, 073006 (2014).
[19] N. Horiuchi, T. Ochiai, J. Inoue, Y. Segawa, Y. Shibata, K. Ishi, Y. Kondo, M. Kanbe, H. Miyazaki, F. Hinode, S. Yamaguti, and K. Ohtaka, Phys. Rev. E **74**, 056601 (2006).
[20] T. Kondo, M. Hangyo, S. Yamaguchi, S. Yano, Y. Segawa, and K. Ohtaka, Phys. Rev. B **70**, 235113 (2004).
[21] S. Yamaguti, J. Inoue, O. Haeberlé, and K. Ohtaka, Phys. Rev. B **66**, 195202 (2002).
[22] P. M. van den Berg, J. Opt. Soc. Am. **63**(12), 1588-1597 (1973).
[23] K. Zhang and D. Li, *Electromagnetic Theory in Microwave and Optoelectronics* (2008), pp. 426-430.
[24] I. G. Tigelis, J. L. Vomvoridis, and S. Tzima, IEEE Trans. Plasma Sci. **26**, 922 (1998).
[25] J. R. Pierce, Proceedings of the IRE **35**, 111 (1947).
[26] A. Bera, R. K. Barik, M. Sattorov, O. Kwon, S.-H. Min, I.-K. Baek, S. Kim, J.-K. So, and G.-S. Park, Opt. Express **22**, 3039 (2014).
[27] CST Corp., CST PS Tutorials. http://www.cstchina.cn/.